37. De Bruyne B, Bartunek J, Sys SU, Pijls NH, Heyndrickx GR, Wijns W. Simultaneous coronary pressure and flow velocity measurements in humans: feasibility, reproducibility, and hemodynamic dependence of coronary flow velocity reserve, hyperemic flow versus pressure slope index, and fractional flow reserve. *Circulation* 1996;94: 1842–1849.
38. Sun KT, Czernin J, Krivokapich J, et al. Effects of dobutamine stimulation on myocardial blood flow, glucose metabolism, and wall motion in normal and dysfunctional myocardium. *Circulation* 1996;94:3146–3154.
39. Zhang J, Path G, Chepuri V, et al. Effects of dobutamine on myocardial blood flow, contractile function, and bioenergetic responses distal to coronary stenosis: implications with regard to dobutamine stress testing. *Am Heart J* 1995;129:330–342.
40. Pierard L, De Landsheere C, Berthe C, Rigo P, Kulbertus H. Identification of viable myocardium by echocardiography during dobutamine infusion in patients with myocardial infarction after thrombolytic therapy: comparison with positron emission tomography. *J Am Coll Cardiol* 1990;15:1021–1031.
41. La Canna G, Alfieri O, Giubbini R, Gargano M, Ferrari R, Visioli O. Echocardiography during infusion of dobutamine for identification of reversible dysfunction in patients with chronic coronary artery disease. *J Am Coll Cardiol* 1994;23:617–626.
42. Severi S, Underwood R, Mohiaddin R, Boyd H, Paterni M, Camici P. Dobutamine stress: effects on regional myocardial blood flow and wall motion. *J Am Coll Cardiol* 1995;126:1187–1195.
43. Forster T, McNeill AJ, Salustri A, et al. Simultaneous dobutamine stress echocardiography and technetium-99m isonitrile single-photon emission computed tomography in patients with suspected coronary artery disease. *J Am Coll Cardiol* 1993;21:1591–1596.
44. Senior R, Sridhara B, Anagnostou E, Handler C, Raftery E, Lahiri A. Synergistic value of simultaneous stress dobutamine sestamibi single-photon-emission computerized tomography and echocardiography in the detection of coronary artery disease. *Am Heart J* 1994;128:713–718.
45. Hoffman R, Lethen H, Kleinhans E, Weiss M, Flachskampf FA, Hanrath P. Comparative evaluation of bicycle and dobutamine stress echocardiography with perfusion scintigraphy and bicycle electrocardiogram for identification of coronary artery disease. *Am J Cardiol* 1993;72:555–559.
46. Marwick TH, D'Hondt AM, Mairesse GH, et al. Comparative ability of dobutamine and stress in inducing myocardial ischaemia in active patients. *Br Heart J* 1994;72: 31–38.
47. Mairesse GH, Marwick TH, Vanoverschelde JL, et al. How accurate is dobutamine stress electrocardiography for detection of coronary artery disease? Comparison with two-dimensional echocardiography and technetium-99m methoxy isobutyl isonitrile (mibi) perfusion scintigraphy. *J Am Coll Cardiol* 1994;24:920–927.
48. Sinusas AJ, Shi QX, Vitols PJ, et al. Impact of regional ventricular function, geometry, and dobutamine stress on quantitative ^{99m}Tc-sestamibi defect size. *Circulation* 1993;88:2224–2234.
49. Kloner R, Allen J, Cox T, Zheng Y, Ruiz C. Stunned left ventricular myocardium after exercise treadmill testing in coronary artery disease. *Am J Cardiol* 1991;68:329–334.
50. Nematzadeh D, Kim YD, Rose JC, Wolf PH, MacNamara TE, Kot PA. Effects of halothane on the intramyocardial pressure of the canine left ventricle. *Cardiovasc Res* 1985;20:275–281.
51. Buljubasic N, Stowe DF, Marijic J, Roerig DL, Kampine JP, Bosajak Z. Halothane reduces release of adenosine, inosine, and lactate with ischemia and reperfusion in isolated hearts. *Anesthesia Analgesia* 1993;73:54–62.
52. Fung A, Gallagher K, Buda A. The physiologic basis of dobutamine as compared with dipyridamole stress interventions in the assessment of critical coronary stenosis. *Circulation* 1987;76:943–951.
53. Calnon DA, Glover DK, Vanzetto G, et al. Dobutamine stress Tc-99m sestamibi uptake underestimates the magnitude of ischemia in dogs with mild and critical coronary stenoses [Abstract]. *J Nucl Med* 1996;37:3P.

Use of Significance Image to Determine Patterns of Cortical Blood Flow Abnormality in Pathological and at-Risk Groups

Alexander S. Houston, Paul M. Kemp, Murdo A. Macleod, T. James R. Francis, Hubert A. Colohan and Helen P. Matthews
Department of Nuclear Medicine, Royal Hospital Haslar, and Department of Undersea Medicine, Institute of Naval Medicine, Gosport; and Department of Psychiatry, University of Southampton, and The Thornhill Unit, Moor Green Hospital, Southampton, United Kingdom

The purpose of this work was to determine whether certain pathological groups and other groups at risk for neurological damage exhibited distinctive patterns of regional cerebral blood flow (rCBF) abnormality. **Methods:** HMPAO SPECT images obtained from six groups of subjects were compared with a normal cortical rCBF atlas, based on multivariate, voxel-by-voxel methods. In each case, a significance image was outputted, highlighting voxels with deficits of ≥3 s.d. of normal. Abnormal patterns were examined for the six groups, which comprised a further 40 normal volunteers, 18 diver controls, 50 divers with decompression illness (DCI), 34 boxers, 23 schizophrenics and 21 subjects with Alzheimer's disease. **Results:** The percentages of abnormal cortical voxels for each group were 0.41%, 0.53%, 1.38%, 1.05%, 0.56% and 2.24%, respectively. The percentages of images in each group with at least one lesion of 10 or more connected abnormal voxels and at least 10 lesions of two or more connected voxels, respectively, were 8% and 8% (normal volunteers), 17% and 11% (diver controls), 38% and 38% (divers with DCI), 41% and 29% (boxers), 26% and 13% (schizophrenics) and 90% and 48% (subjects with Alzheimer's disease). This suggests that multiple small lesions are as common as single large lesions for divers with DCI but not for patients with Alzheimer's disease or schizophrenia. Large lesions are located predominantly in the parietal and inferior temporal regions for Alzheimer's disease, in the parietal and occipital regions for divers with DCI and boxers and in the inferior frontal region for schizophrenia. **Conclusion:** It appears that the groups considered here do have different rCBF patterns and that the significance image is a useful way of demonstrating this fact.

Key Words: regional cerebral blood flow; decompression illness; boxing; schizophrenia; Alzheimer's disease

J Nucl Med 1998; 39:425–430

Previously, a method was described for determining the significance of abnormalities in a regional cerebral blood flow (rCBF) SPECT image using a normal atlas built from a mean and several principal component (PC) images from a database of normal control subjects (*1*). This method has since been optimized for differentiating further normal control subjects from patients with dementia (*2*). This study represents an application of this work to certain pathological groups of subjects and other groups of subjects considered to be at risk for neurological damage.

The groups examined were:

1. Normal controls;
2. Undersea divers with no history of decompression illness (DCI);
3. Undersea divers with DCI;
4. Amateur boxers;
5. Schizophrenics; and

Received Nov. 25, 1996; revision accepted Jun. 16, 1997.
For correspondence or reprints contact: Alexander S. Houston, PhD, Department of Nuclear Medicine, Royal Hospital Haslar, Gosport, Hants, PO12 2AA, United Kingdom.

6. Subjects with Alzheimer's disease.

In each case, the subjects were selected for research testing according to specific criteria and, apart from divers with DCI who were admitted after accidents, they were not merely referred to the Department of Nuclear Medicine as patients.

MATERIALS AND METHODS

Database of Normal Images

To set ranges of normality, it is first necessary to collect a reference database of normal images. It is important that this database is sufficiently large and varied to form a representative sample of the normal population. Often, this is not possible due to ethical considerations, and some degree of compromise is necessary.

As an example, rCBF SPECT images were obtained from 50 normal volunteers (30 men, 20 women; age range 18–58 yr; median age = 28 yr). Strict exclusion criteria were applied in their selection, including no history of neurological disease, no previous head injuries involving concussion and no active participation in boxing or undersea diving (*3*).

The acquisition and reconstruction procedure was as previously defined (*1*), involving an intravenous injection of 600 MBq of ^{99m}Tc-HMPAO; acquisition of images of 64 × 64 matrix size at 64 projections using a gamma camera (Siemens ZLC7500)/computer (Park Medical MICAS V) system; and filtered backprojection using a soft Shepp-Logan filter, resulting in image matrices of 64 × 64 × 64. These were subsequently zoomed to 32 × 32 × 32 matrices without loss of relevant information. Voxels were cubic, with a side length equal to 0.64 cm.

Preprocessing

Before an atlas can be formed, it is necessary to align these images using some form of image coregistration. Because rescaling during the processing stage can lead to problems (*2*), it is also necessary to scale the images at this stage. Currently, it is thought that scaling to global values is the best solution.

For the rCBF example, a reference image was selected from the normal database and all other images registered with respect to it using a three-dimensional affine transform with 12 degrees of freedom because this was considered appropriate for low-resolution SPECT images. Specifically, a coordinate transfer function $\{a_{ij}\}$ from (x,y,z) space to (r,s,t) space was determined such that:

$$r = a_{11} + a_{12}x + a_{13}y + a_{14}z,$$

$$s = a_{21} + a_{22}x + a_{23}y + a_{24}z,$$

$$t = a_{31} + a_{32}x + a_{33}y + a_{34}z.$$

The method was fully automatic and was based on the concept of optic flow developed by Horn and Schunck (*4*). A detailed mathematical description of the method and its application to SPECT images is provided by Barber et al. (*5,6*), who also measured the accuracy of the technique for HMPAO images of a similar nature to those used here. They concluded that the method was appropriate for such images, although it is possible that this conclusion may not extend to high-resolution images.

Because the cortical region alone was considered, scaling was to global counts in this region with respect to the reference image. The cortical region was defined on the reference image by a nuclear medicine physician. A two-dimensional region corresponding to cortex was drawn carefully using a number cluster keypad on each axial section considered by the physician to include cortex. Sixteen such sections were used, and the three-dimensional cortical region thus formed involved a total of 5,892 voxels. Because all images were first registered with respect to the reference image, the defined region could be superimposed on each registered image.

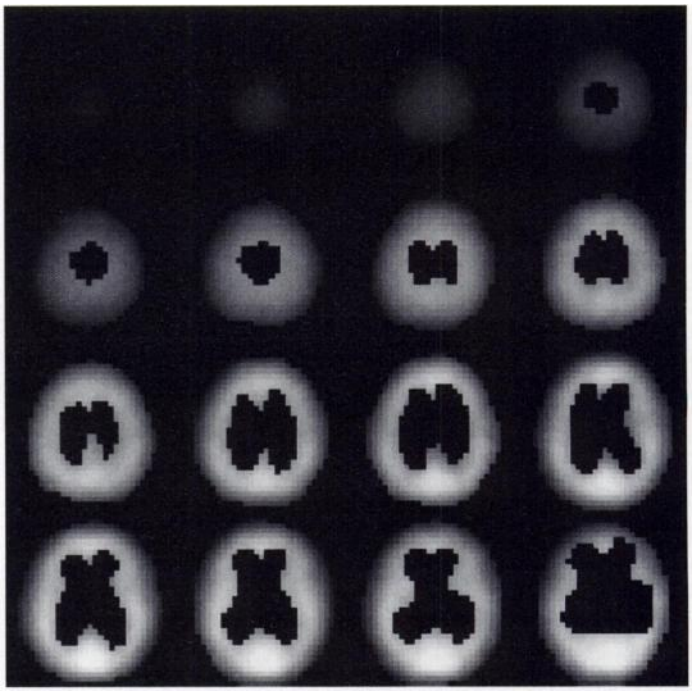

FIGURE 1. The axial sections of the mean cortical image of the normal atlas are shown. The sections are depicted from top to bottom, left to right, starting at the top of the brain.

A ratio of cortical count density to cerebellar count density was also obtained because the latter region is considered to be fairly stable in most, but not all, pathologies. There was some concern that, if this ratio was sufficiently low, a uniformly reduced rCBF in the cortex, when normalized to global cortical counts, would be interpreted as normal. A normal range for this ratio was established using values obtained from the reference database, and subsequent images with reduced ratios outside the lower limit were examined.

Construction of Normal Atlas

A normal atlas was then formed from the database of normal images consisting of a mean image, several PC images and a residual s.d. image (*1*). To obtain these, a PC analysis was performed on the cortical region of the images using the voxel as a variable. The resulting components may be displayed as PC images, which represent patterns of correlated normal variation within the database of normal images. The factor loadings or coefficients represent the positive or negative contribution of each PC image to each original image.

The number of PC images to be used will depend on the type of image being considered. The coefficients of the PC images for the normal reference set were normalized so that they represented numbers of s.d. of their own range. This is possible because there exists one available degree of freedom involving the respective scaling of coefficients and PC images.

Four PC images were used for the normal rCBF atlas because this number was shown to give optimal differentiation between normal controls and patients with dementia (*2*). A fuller description of this trial appears later. The first four eigenvalues account for 9.3%, 7.1% (cumulative 16.4%), 5.8% (22.2%) and 5.1% (27.3%) of the total variance in the images. It has been shown that noise alone accounts for around 54% of the variance in these images (*7*). The mean image and first PC image are shown in Figures 1 and 2, respectively. Note that all voxels outside the cortical region have been masked by the procedure.

Analysis of Subsequent Images

For subsequent images, a nearest normal equivalent (NNE) image was obtained automatically from the normal atlas by adding

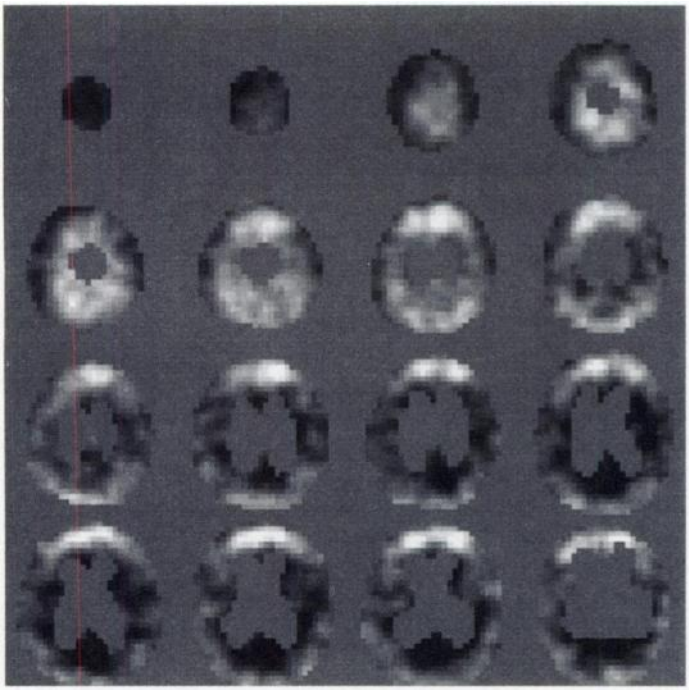

FIGURE 2. The axial sections of the first cortical PC image of the normal atlas are shown. The sections are depicted from top to bottom, left to right, starting at the top of the brain. The background gray level represents a value of zero. Positive and negative values are depicted as brighter and darker, respectively, than the background level.

the mean image to a linear combination of the PC images (*1*). The coefficient for each PC image was calculated by representing the new image as a vector, subtracting from it the mean image vector of the normal atlas and forming the scalar product of the resultant vector with the appropriate component. The result was then divided by the sum of squares of the elements of the component. This follows directly from the orthogonal properties of PCs. In the construction of the NNE image, the coefficients were constrained to lie within a normal range. This is necessary because coefficients are meant to represent degrees of normal deviation from the mean image of the atlas. Clearly, there is a danger that, in certain circumstances, very large coefficients might represent abnormality.

The NNE image was compared with the original and positive and negative difference images formed. These were then compared with the residual image, and significance images were obtained, corresponding alternatively to positive and negative differences and measured in numbers of s.d. All calculations are performed at the voxel level.

For the SPECT example, coefficients outside the range [−3,3] were set to these limits. This ensures that the coefficients are within ±3 s.d. of the normal range. For rCBF, only regions of count deficiency were considered to be important. Hence, a single significance image was required, corresponding to count deficient voxels in the original image.

Analysis of Coefficients

The rationale behind the method was that, because only normal studies were used to construct the atlas, coefficients will represent normal deviation from the mean normal image. As such, they should not relate directly to abnormality.

Although it is not the subject of this study to relate components to variables such as age and sex, it is interesting to examine the possibility that such relationships exist. For this purpose, a multivariate general linear model with type III sum of squares (SPSS Advanced Statistics, version 7.5) was performed on the normal reference set, using the unconstrained coefficients of the four components as dependent variables, sex as a fixed factor and age as a covariate.

Although it was not expected that the coefficients will relate directly to abnormality, it was possible that they related indirectly through a covariate such as age. For instance, if an abnormal pattern is related to the aging process, this pattern may present itself among a normal population with a large age range. This is why the coefficients of the model were constrained to lie within ±3 s.d. of the normal range. To test the extent of this problem, the number of subjects in each group requiring such a constraint on at least one coefficient was calculated.

Thresholding

Thresholding by s.d. was performed on the significance image to define whether or not a voxel should be classed as abnormal. This thresholding produced an image with binary elements.

Clearly, in a three-dimensional image containing many voxels, there will be several apparently abnormal voxels occurring by chance. It is unlikely, however, that many connected abnormal voxels, e.g., as in a real lesion, will be due to a chance finding. This suggests that thresholding the number of connected abnormal voxels is necessary to define a lesion in the image. This will vary, not only with the type of image but also with the suspected pathology being investigated.

In a previous study involving images of 40 normal controls and 200 patients with dementia (*2*), receiver operating characteristic curves were generated using the s.d. threshold as the variable for different values of other parameters, such as the number of components and the threshold number of connected voxels. The area under the receiver operating characteristic curve was maximized when four components were used, together with a threshold of around 10 connected voxels. An acceptable false-positive rate, i.e., less than 10%, was obtained for this value using an s.d. threshold of 3 (*2*), although this rate is clearly greater than a chance finding. These values were adopted in the current study.

Location Masking

It is usually of great importance to determine the location of any suspected lesions in an image. This may be done by visual inspection of the significance image. Alternatively, a registered image may be divided into appropriate regions by a physician. These regions may then be used to mask the s.d. threshold image and result in output for each location. This latter approach is more appropriate for cases in which patterns of abnormality are sought in a database of images corresponding to a particular pathology.

For rCBF images, mutually exclusive regions corresponding to left frontal (LF) and right frontal (RF), left parietal (LP) and right parietal (RP), left inferior frontal (LIF) and right inferior frontal (RIF), left inferior temporal (LIT) and right inferior temporal (RIT) and occipital region (OR) were defined by a nuclear medicine physician on the reference image in the normal database. These regions are shown in Figure 3.

Pathological and at-Risk Groups

The groups studied were as follows.

Normal Controls. A further 40 normal controls, subject to the same exclusion criteria as before, were imaged for rCBF. Because these were chosen primarily to be matched against boxers, they were all men (age range 18–29 yr; median age = 22 yr).

Undersea Divers. Eighteen undersea divers, with no history of DCI, were imaged as part of a case–control study of the effect of DCI on rCBF (*8*). The group included 1 woman and 17 men (age range 26–59 yr; median age = 38 yr), and participation in diving ranged from novice (<30 dives) to experienced (>300 dives) divers.

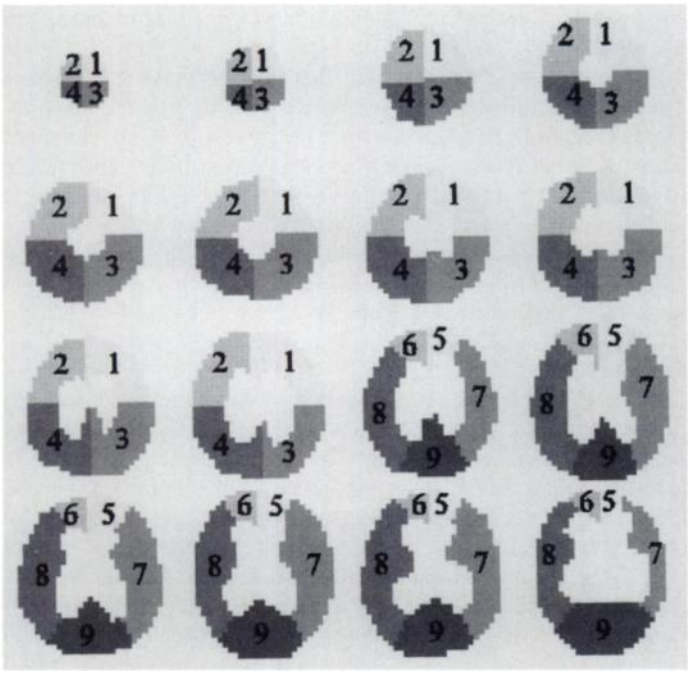

FIGURE 3. The regions corresponding to LF (1), RF (2), LP (3), RP (4), LIF (5), RIF (6), LIT (7), RIT (8) and OR (9) are shown for each axial section of the cortex.

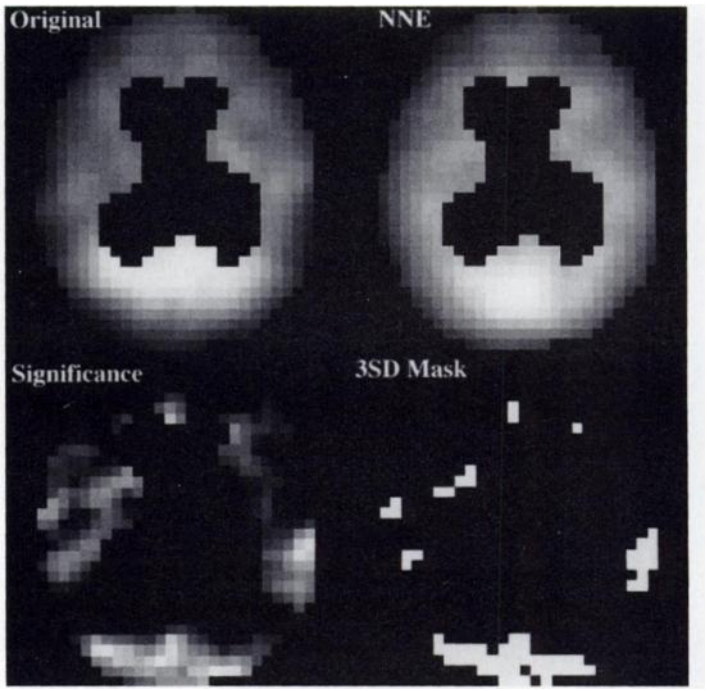

FIGURE 4. The original image, the NNE image, the significance image and the 3 s.d. masked image are shown for a single axial section of the cortex for a subject with Alzheimer's disease.

Divers with DCI. Fifty divers suffering from DCI were imaged for rCBF both as part of and subsequent to the aforementioned case–control study (*9*). Dysbarism, giving rise to DCI, is caused by an uncontrolled rapid ascent to the surface from depths beyond 10 m, resulting in a massive release of gas bubbles, from nitrogen in solution, due to rapid decompression. These bubbles produce gas emboli, which give rise to clinically manifest signs and symptoms, e.g., sensory loss, numbness, tingling, pain in joints, motor weakness and cerebral cortical perfusion defects, on SPECT imaging (*10*). Other possible causes of perfusion abnormalities, e.g., trauma, cerebrovascular disease, dementia and so on, can be elicited by detailed history-taking or, if serious enough to have given rise to clinical signs and symptoms, would have been apparent at compulsory diving medical examinations.

The divers were brought to a compression chamber as soon as possible (generally within hours) after the onset. They were examined by the duty diving medicine specialist before recompression and controlled decompression. They were injected with ^{99m}Tc-HMPAO, before recompression if possible, and imaged in the Department of Nuclear Medicine. The group included 5 women and 45 men (age range 15–56 yr; median age = 29).

Amateur Boxers. Thirty-four boxers were imaged as part of a study into the effects of boxing on rCBF (*3*). These were amateur boxers who represented either the Royal Navy or British Army at the time of request. None of the boxers had sustained a relevant head injury outside the ring (defined as more than momentary loss of consciousness or concussion lasting more than a minute) or had a history of neurological illness. Although it is not possible to remove entirely the potentially confounding factor of concurrent drug abuse, it should be emphasized that all 34 boxers, as well as many members of the normal control and both diving groups, were service personnel. As such, it is hoped that any confounding variables would be common to all of these groups. Drug abuse is an extremely serious offense in the British forces and results in dismissal. It is strongly believed that the prevalence of drug abuse in British Service personnel is less than in their civilian counterparts.

All boxers in the group were men, the age range was 18–29 yr (median age = 20 yr), and the duration of participation in boxing was between 3 mo and 17 yr, involving up to 250 bouts (median = 40 bouts).

Schizophrenics. Twenty-three schizophrenics were referred to the Department of Nuclear Medicine, Royal Hospital Haslar, and imaged so that rCBF patterns could be examined. These patients were chosen from consecutive patients in contact with the psychiatric services in three hospitals (Park Prewett Hospital, Royal South Hants Hospital and Knowle Hospital) in the Wessex region of England. If, on case note review, these patients appeared likely to fulfill the DSM-III-R criteria for schizophrenia (*11*), they were invited to attend a clinical interview to confirm the diagnosis and to assess the severity of symptomatology. Exclusion criteria were: previous history of organic psychiatric disorder, mental handicap, epilepsy, head injury, substance abuse, cerebrovascular disease, neurological disorder and use of psychotropic medication other than neuroleptics and antichlorinergics in the previous 2 mo. Symptomatology was recorded using the Present State Examination (ninth edition) (*12*). The group included 6 women and 17 men, and the age range was 20–68 yr (median age = 35 yr).

Subjects with Alzheimer's Disease. Twenty-one subjects classified as suffering from "probable Alzheimer's disease" under the National Institute of Neurological and Communicative Disorders and Stroke–Alzheimer's Disease and Related Disorders Association classification (*13*) had rCBF images taken before and after drug treatment. A full screen designed to identify secondary causes of dementia was performed (*14*). Patients with significant renal or hepatic dysfunction, blood dyscrasias or any intercurrent serious physical illness were excluded. In this study, the images taken before treatment were used to examine patterns of abnormality. The group included 11 women and 10 men and the age range was 60–84 yr (median = 79 yr).

RESULTS

An axial section of an image of a subject with Alzheimer's disease is shown together with the corresponding section of its NNE image in Figure 4. Also shown are the corresponding significance and s.d. threshold sections.

TABLE 1
Percentages of Abnormal Voxels in Each Region

	Region									
	Cortex	LF	RF	LP	RP	LIF	RIF	LIT	RIT	OR
Reference set	0.07	0.06	0.03	0.07	0.10	0.08	0.03	0.10	0.09	0.05
Normals	0.41	0.31	0.36	0.29	0.15	0.31	0.33	0.52	0.49	0.83
Divers	0.53	0.38	0.45	0.56	0.52	0.41	0.52	0.58	0.62	0.60
DCI	1.38	1.42	0.82	1.62	1.48	1.47	0.62	1.16	1.11	2.35
Boxers	1.05	0.57	0.55	1.04	1.37	1.13	0.87	1.09	1.14	1.66
Schizophrenia	0.56	0.51	0.49	0.43	0.60	1.43	1.24	0.57	0.48	0.46
Alzheimer's disease	2.24	1.52	2.20	1.98	2.28	4.01	3.06	2.57	1.57	3.05

The percentages of abnormal voxels in the cortex and each of its subdivisions are shown for each group in Table 1.

The numbers of studies with at least 1 lesion of 10 or more connected voxels, at least three lesions of five or more connected voxels and at least 10 lesions of 2 or more connected voxels in the cortex are shown for each group in Table 2.

The number of studies with at least one lesion of 10 or more connected voxels contained within a given sector is shown for each group in Table 3. Note that numbers of subjects with at least one large lesion do not sum to the value shown in Table 2 because a single subject may have multiple large lesions in several sectors. Also, a large lesion across a sector boundary might split to give a large lesion in both sectors, a large lesion in one of the sectors or no large lesion in either sector.

The normal range for cortex–cerebellum count density ratios, based on 2 s.d. on either side of the mean, was found to be 0.610–0.723. Three subjects in all categories had values of <0.610, including one diver control (0.608) and two subjects with Alzheimer's disease (both 0.600), all with values above the 3 s.d. lower limit of 0.581. Both Alzheimer's subjects were classified as abnormal by each of the three criteria used in Table 2, whereas the diver control was classified as abnormal by the two criteria involving greater than five connected voxels.

Using the multivariate general linear model with the Wilks' lambda statistic to analyze the unconstrained coefficients of the normal reference set for the four components, we found that age was a significant covariate ($p < 0.05$), whereas sex was not a significant factor ($p > 0.2$). Univariate tests of between-subject effects revealed that age was a significant effect for the first component only ($p < 0.05$).

The number of subjects within each group who had one or more coefficients originally outside the normal range [−3,3] were as follows: reference normal controls (1 of 50); further normal controls (0 of 40); diver controls (0 of 18); divers with DCI (2 of 50); boxers (1 of 34); schizophrenics (1 of 23); and subjects with Alzheimer's disease (1 of 21). Although there is a tendency for the odd individual in the pathological and at-risk groups to require coefficient constraint, there is nothing to suggest that this is a serious problem.

TABLE 2
Number of Studies Deemed Abnormal by Each Criterion

		Criterion		
	No.	1 lesion/ 10 voxels	3 lesions/ 5 voxels	10 lesions/ 2 voxels
Reference set	50	0	0	0
Normals	40	3	4	3
Divers	18	3	3	2
DCI	50	19	20	19
Boxers	34	14	10	10
Schizophrenia	23	6	4	3
Alzheimer's disease	21	19	16	10

DISCUSSION

The importance of having a representative reference set has already been stated. Clearly, the selection of normal controls used for validation is from a different population, regarding age and sex distribution, than those used for the reference set. Nevertheless, differences in the detection of abnormalities between these two groups shown in Tables 1–3 suggest that a reference set of 50 normal images is too small. Due to ethical and radiation protection considerations, large reference sets are not practical at the current time.

Tables 1 and 2 show clearly that some of the groups (subjects with Alzheimer's disease, divers with DCI and boxers) are much more likely to provide an abnormal result than the others, based on the criteria used here.

Using a chi-square test with Yates' correction on the results shown in Table 2, the incidence of at least one large (≥10 voxels) lesion was increased significantly in subjects with Alzheimer's disease (chi-square = 37.6; $p < 0.001$), divers with DCI (chi-square = 9.6; $p < 0.005$) and boxers (chi-square = 10.0; $p < 0.005$), with respect to the 40 normal controls. The incidence of at least three medium (≥5 voxels) lesions was increased significantly in subjects with Alzheimer's disease (chi-square = 24.5; $p < 0.001$) and divers with DCI (chi-square = 8.8; $p < 0.005$) but not in boxers (chi-square = 3.3; $p > 0.05$). The incidence of at least 10 small (≥2 voxels) lesions was increased significantly in subjects with Alzheimer's disease (chi-square = 10.9; $p < 0.001$), divers with DCI (chi-square = 9.6; $p < 0.005$) and boxers (chi-square = 4.7; $p < 0.05$). The incidence of large or medium or small lesions was not increased significantly in schizophrenics or diver controls ($p > 0.05$).

Table 2 shows also that the incidence of multiple small lesions was as great as the incidence of at least one large lesion for divers with DCI but not for subjects with Alzheimer's disease. This is consistent with the findings of Staff et al. (*10*), who used texture analysis on similar images and reported coarsely patchy rCBF patterns in divers with DCI.

Table 3 shows that large lesions are located predominantly in the parietal and inferior temporal regions for Alzheimer's disease and in the parietal and occipital regions for divers with DCI and boxers. The results for subjects with Alzheimer's disease are consistent with the findings of other researchers (*15–22*), thereby generating some confidence in the use of the method.

There is some evidence that schizophrenics may have abnormal rCBF patterns, but this is not conclusive. Previous research on schizophrenics (*23,24*) has indicated blood flow deficiencies

TABLE 3
Number of Studies with at Least One Large (10 Voxels) Lesion in Each Region

		Region								
	No.	LF	RF	LP	RP	LIF	RIF	LIT	RIT	OR
Reference set	50	0	0	0	0	0	0	0	0	0
Normals	40	0	0	1	0	0	0	1	0	2
Divers	18	0	0	2	0	0	0	0	0	1
DCI	50	4	4	6	6	4	1	6	3	7
Boxers	34	1	1	4	4	2	0	3	3	7
Schizophrenia	23	0	0	1	1	1	2	1	2	2
Alzheimer's disease	21	3	6	7	10	3	3	10	6	5

in the frontal lobes. Table 1 provides some corroborative evidence of this finding, particularly in the inferior frontal regions. Similarly, although divers with no history of DCI have slightly higher percentages of abnormal voxels and 10-voxel lesions, there is insufficient statistical evidence to prove that this is a real effect.

Problems with the technique at present include the representative nature of the normal reference set; the need for different reference sets from center to center and from imaging device to imaging device within a center; and the normalization to global values when this parameter, in itself, may contribute to the diagnostic process. The first of these can only be answered with a better understanding of the risks involved and the trade-off with having an inadequate reference population; the second requires better standardization of device and method between centers; whereas the third may involve combining the use of the method with a ratio of global values to values obtained from a reference region unaffected by pathology. In this study, significantly reduced cortex–cerebellum count density ratios were found rarely and, when found, did not affect classification using most of the adopted criteria, although any subsequent estimation of severity of abnormality may have been reduced.

Another problem specific to this analysis is the choice of further normal controls for comparison purposes. Clearly, it would be advantageous to have sex- and age-matched controls for each pathological and at-risk group, particularly because the first component may be related to age. Again, this is not possible for ethical reasons due to the numbers and age range required to handle disparities between groups, such as amateur boxers and subjects with Alzheimer's disease.

Although it is an implicit assumption of the adopted approach that the normal reference set is sufficiently representative of the normal population to yield a stable normal atlas, no implicit statistical assumption is made regarding individuals in the pathological and at-risk groups, other than that they are indicative of their group. Any conclusions drawn should therefore be viewed with this in mind. Neither is the assumption made that differential patterns actually exist between these groups and the normal population. Other techniques, such as discriminant analysis, actively seek such patterns and, when used subsequently as a classifier, assume that the groups have been sampled in a representative manner, an exercise that is nearly impossible for abnormal groups. It is precisely for this reason that the current approach was adopted.

CONCLUSION

The significance image, as defined here, appears to be a useful way of assessing suspected abnormalities in medical images. As demonstrated in the example considered, it may be used with apparent success to determine patterns of abnormality in different pathological and at-risk groups.

Large rCBF abnormalities are detected in the great majority of subjects with Alzheimer's disease, whereas divers with DCI and boxers also have a significantly increased incidence of such abnormalities with respect to normal controls. The incidence of multiple small lesions is as great as single (or multiple) large lesions in divers with DCI. Schizophrenics and divers with no history of DCI appear to have a raised incidence of large lesions, although this was not statistically significant here.

ACKNOWLEDGMENTS

We thank Professor David C. Barber of the Royal Hallamshire Hospital (Sheffield, United Kingdom) for the use of his computer program for image registration.

REFERENCES

1. Houston AS, Kemp PM, Macleod MA. A method for assessing the significance of abnormalities in HMPAO brain SPECT images. *J Nucl Med* 1994;35:239–244.
2. Houston AS, Kemp PM, Macleod MA. Optimization of factors affecting the state of normality of a medical image. *Phys Med Biol* 1996;41:755–765.
3. Kemp PM, Houston AS, Macleod MA, Pethybridge RJ. Cerebral perfusion and psychometric testing in military amateur boxers and controls. *J Neurol Neurosurg Psychiatry* 1995;59:368–374.
4. Horn BKP, Schunck BG. Determining optic flow. *Artif Intell* 1981;17:185–203.
5. Barber DC. Registration of low resolution images. *Phys Med Biol* 1992;37:1485–1498.
6. Barber DC, Tindale WB, Hunt E, Mayes A, Sagar HJ. Automatic registration of SPECT images as an alternative to immobilization in neuroactivation studies. *Phys Med Biol* 1995;40:449–463.
7. Houston AS, Kemp PM, Griffiths PT, Macleod MA. An estimation of noise levels in HMPAO rCBF SPECT images using simulation and phantom data; comparison with results obtained from repeated normal controls. *Phys Med Biol* 1994;39:873–884.
8. Hodgson M, Smith DJ, Macleod MA, Houston AS, Francis TJR. Case control study of cerebral perfusion deficits in divers using ^{99m}Tc hexamethyl-propylene amine oxime. *Undersea Biomed Res* 1991;18:421–431.
9. Macleod MA, Houston AS, Kemp PM, Francis TJR. A voxel by voxel multivariate analysis of cerebral perfusion defects in divers with "bends". *Nucl Med Commun* 1996;17:795–798.
10. Staff RT, Gemmell HG, Duff PM, et al. Decompression illness in sports divers detected with technetium-99m-HMPAO SPECT and texture analysis. *J Nucl Med* 1996;37:1154–1158.
11. American Psychiatric Association. *Diagnostic and statistical manual of mental disorders*, 3rd ed., revised. Washington, D.C.: American Psychiatric Association; 1987.
12. Wing JK, Cooper JE, Sartorius N. *The measurement and classification of psychiatric symptoms*. New York: Cambridge University Press; 1974.
13. McKhann G, Drachman D, Folstein M, Katzman R, Price D, Stadlan EM. Clinical diagnosis of Alzheimer's disease: report of NINCDS-ADRDA Work Group under the auspices of the Department of Health and Human Services Task Force on Alzheimer's disease. *Neurology* 1984;34:939–944.
14. Philpot MP, Levy R. A memory clinic for the early diagnosis of dementia. *Int J Geriatr Psychiatry* 1987;2:195–200.
15. Gemmell HG, Sharp PF, Besson JA, et al. Differential diagnosis in dementia using the cerebral blood flow agent ^{99m}Tc HMPAO: a SPECT study. *J Comput Assist Tomogr* 1987;11:398–402.
16. Launes J, Sulkava R, Erkinjuntti T, et al. Technetium-99m-HMPAO SPECT in suspected dementia. *Nucl Med Commun* 1991;12:757–765.
17. Holman BL, Johnson KA, Gerada B, Carvalho PA, Satlin A. The scintigraphic appearance of Alzheimer's disease: a prospective study using technetium-99m-HMPAO SPECT. *J Nucl Med* 1992;33:181–185.
18. Jobst KA, Smith AD, Barker CS, et al. Association of atrophy of the medial temporal lobe with reduced blood flow in the posterior parietotemporal cortex in patients with a clinical and pathological diagnosis of Alzheimer's disease. *J Neurol Neurosurg Psychiatry* 1992;55:190–194.
19. Wyper D, Teasdale E, Patterson J, et al. Abnormalities in rCBF and computed tomography in patients with Alzheimer's disease and in controls. *Br J Radiology* 1993;66:23–27.
20. Claus JJ, van Harskamp F, Breteler MMB, et al. Assessment of cerebral perfusion with single-photon emission tomography in normal subjects and in patients with Alzheimer's disease: effects of region of interest selection. *Eur J Nucl Med* 1994;21:1044–1051.
21. Mielke R, Pietrzyk U, Jacobs A, et al. HMPAO SPECT and FDG PET in Alzheimer's disease and vascular dementia: comparison of perfusion and metabolic pattern. *Eur J Nucl Med* 1994;21:1052–1060.
22. Page MPA, Howard RJ, O'Brien JT, Buxton-Thomas MS, Pickering AD. Use of neural networks in brain SPECT to diagnose Alzheimer's disease. *J Nucl Med* 1996;37:195–200.
23. Erbas B, Kumbasar H, Erbengi G, Bekdik C. Tc-99m HMPAO/SPECT determination of regional cerebral blood flow changes in schizophrenics. *Clin Nucl Med* 1990;15:904–907.
24. Lewis SW, Ford RA, Syed GM, Reveley AM, Toone BK. A controlled study of ^{99m}Tc-HMPAO single-photon emission imaging in chronic schizophrenia. *Psychol Med* 1992;22:27–35.